ELSEVIER

Vibrational Spectroscopy 7 (1994) 149–162

VIBRATIONAL SPECTROSCOPY

Infrared study of styrene oxide and phenylacetylene in various solutions

Richard A. Nyquist *, Steve Fiedler

Analytical Sciences Laboratory, 1897F Building, Dow Chemical Company, Midland, MI 48667, USA

(Received 8th November 1993)

Abstract

The epoxy ring breathing mode and epoxy asymmetric deformation increase in frequency while the epoxy symmetric deformation for styrene oxide decreases in frequency as the mole% $CHCl_3/CCl_4$ or $CDCl_3/CCl_4$ increases. The ν(≡C–H), ν(C≡C) and ν_{24} (b_1) modes for phenylacetylene decrease in frequency while the δ_{ip}(≡C–H), γ_{op}(≡C–H), ν_{32} (b_2) and ν_{34} (b_2) modes increase in frequency for phenylacetylene as the mole% $CHCl_3/CCl_4$ increases. The modes associated with the acetylenic group change more in frequency with change in the solvent than do the phenyl ring modes. There is a linear relationship between the change in the δ_{ip}(≡C–H) and γ_{op}(≡C–H) frequencies for phenylacetylene with change in the solvent system. The changes in the epoxy group frequencies and the acetylenic group frequencies with change in the solvent system indicate that these functional groups form complexes with the solvent system. Intermolecular hydrogen bonded complexes and dipolar effects are given as the major factors in affecting the discussed group frequency changes with changes in the solvent system.

Key words: Infrared spectrometry; Epoxy ring; Hydrogen bonds; Solvent effects;

1. Introduction

The characteristic ring modes for the epoxy ring, —CH(O)—CH_2, for ethylene oxide, 1,2-epoxyalkanes, and the epihalohydrins are summarized in Table 1. Comparable modes for styrene oxide are observed near 1251, 985, and 878 cm^{-1}. Vibrational assignments for phenylacetylene (also named ethynylbenzene) have been made [4]. The characteristic vibrational frequencies for the –C≡C–H group for phenylacetylene are as follows: ν(≡C–H), 3315 cm^{-1} (CCl_4 solution); ν(C≡C), 2119 cm^{-1} (CCl_4 solution); δ_{ip}(≡C–H), 648 cm^{-1} (CS_2 solution); γ_{op}(≡C–H), 610 cm^{-1} (CS_2 solution).

We have studied the solvent effects on group frequencies for a variety of chemical compounds [5–28], and the study of styrene oxide and phenylacetylene in various dilute solutions or in $CHCl_3/CCl_4$ solvents is an extension of our interest in solute–solvent interactions.

* Corresponding author.

SSDI 0924-2031(94)00013-7

Table 1
Characteristic epoxy ring modes (in cm^{-1})

Mode	Ethylene oxide [1]	1,2-Epoxy alkane [2]	Epihalohydrin [3]				
			F	Cl	Br	I	
Ring breath	1270.5	1248–1268	1257.4	1254.8	1256.1	1260	R_1
			–	1266.8	1262.0	1253	RT
Antisymmetric deformation	897	883– 932	906.4	905.8	888.2	911	R_1
	877	830– 877	860.0	854.0	845.8	841	R_1
			838.2	845.0	833.2	862	RT

2. Experimental

Infrared (IR) spectra were recorded with the use of a Nicolet 605X-FT-IR system. The samples were prepared as 2 wt.% solutions in $CHCl_3$ (or $CDCl_3$) and CCl_4 solutions and in other solvents. The stock $CHCl_3$ (or $CDCl_3$) and CCl_4 solutions of phenylacetylene and styrene oxide were used to prepare the various mole% $CHCl_3$ (or $CDCl_3$)/CCl_4 solutions listed in Tables 2 and 3. All spectra were recorded using a 0.1 mm KBr cell. The IR spectra were recorded using 4 cm^{-1} resolution, and the data included in this report are those peak-picked by the computer.

3. Results and discussion

3.1. Styrene oxide

The $CDCl_3$/CCl_4 solution data and the $CHCl_3$/CCl_4 solution data for styrene oxide are

Table 2
IR data for styrene oxide in $CDCl_3$ and/or CCl_4 solutions

Mole% $CDCl_3$/CCl_4	Antisymmetric deformation cm^{-1}	Ring breath cm^{-1}
0.00	984.82	1252.40
10.74	985.06	1252.64
19.40	985.12	1252.70
26.53	985.18	1252.75
32.50	985.23	1252.79
37.57	985.27	1252.81
41.93	985.29	1252.83
45.73	985.32	1252.86
49.06	985.32	1252.86
52.00	985.36	1252.90
54.62	985.36	1252.90
57.22	985.39	1252.93
60.07	985.39	1252.93
63.28	985.40	1252.95
66.73	985.42	1252.97
70.65	985.44	1253.00
75.06	985.46	1253.05
80.06	985.48	1253.09
85.05	985.50	1253.18
92.33	985.52	1253.27
100.00	985.55	1253.46
Δcm^{-1}	0.73	1.06

Table 3
IR data for styrene oxide in $CHCl_3$ and/or CCl_4 solutions

Mole% $CHCl_3$/CCl_4	Symmetric deformation cm^{-1}	Antisymmetric deformation cm^{-1}
0.00	879.230	984.830
10.74	878.890	984.910
19.40	878.680	984.940
26.53	878.480	985.000
32.50	878.340	985.040
37.57	878.260	985.050
41.93	878.180	985.080
45.73	878.110	985.090
49.06	878.050	985.110
52.00	878.000	985.126
54.62	877.949	985.132
57.22	877.527	985.294
60.07	877.596	985.268
63.28	877.666	985.237
66.73	877.720	985.217
70.65	877.781	985.189
75.06	877.831	985.174
80.06	877.884	985.156
85.05	877.929	985.143
92.33	877.990	985.120
100.00	877.430	985.350
Δcm^{-1}	−1.80	0.52

Table 4
Infrared data (in cm^{-1}) for phenyl acetylene in $CHCl_3$ and/or CCl_4 solutions

Mole% $CHCl_3/CCl_4$	ν(≡C–H)	ν(C≡C)	δ_{ip}(≡C–H)	γ_{op}(≡C–H)	ν_{32} (b_2) ring def	ν_{34}(b_2) sk def	ν_{24} (b_1) sk def
0.00	3313.10	2112.95	650.42	613.79	690.37	530.04	513.55
10.74	3312.32	2112.21	651.29	615.01	690.47	530.14	513.51
19.40	3312.00	2111.84	651.70	615.62	690.53	530.18	513.47
26.53	3311.71	2111.68	652.00	616.47	690.59	530.21	513.47
32.50	3311.47	2111.56	652.28	617.54	690.64	530.24	513.45
37.57	3311.32	2111.47	652.48	619.89	690.69	530.26	513.47
41.93	3311.19	2111.37	652.72	620.54	690.74	530.28	513.41
45.73	3311.03	2111.22	653.05	621.22	690.80	530.29	513.42
49.06	3310.97	2111.21	653.20	621.42	690.83	530.30	513.43
52.00	3310.90	2111.12	653.42	621.73	690.85	530.31	513.40
54.62	3310.89	2111.12	653.45	621.82	690.86	530.31	513.38
57.22	3310.87	2111.08	653.50	621.82	690.87	530.31	513.39
60.07	3310.73	2111.00	653.85	622.16	690.93	530.32	513.38
63.28	3310.37	2110.68	–	622.11	691.09	530.35	513.37
66.73	3310.52	2110.83	–	622.49	691.02	530.34	513.37
70.65	3310.37	2110.68	–	622.65	691.09	530.35	513.37
75.06	3310.21	2110.54	–	622.85	691.17	530.36	513.35
80.06	3310.01	2110.40	–	623.03	691.27	530.38	513.33
85.05	3309.21	2110.21	–	623.22	691.38	530.39	513.33
92.33	3309.41	2109.97	–	623.56	691.57	530.42	513.33
100.00	3309.05	2109.78	–	624.18	691.83	530.48	513.39
Δcm^{-1}	−4.05	−3.17	3.43	10.39	1.46	0.44	−0.24

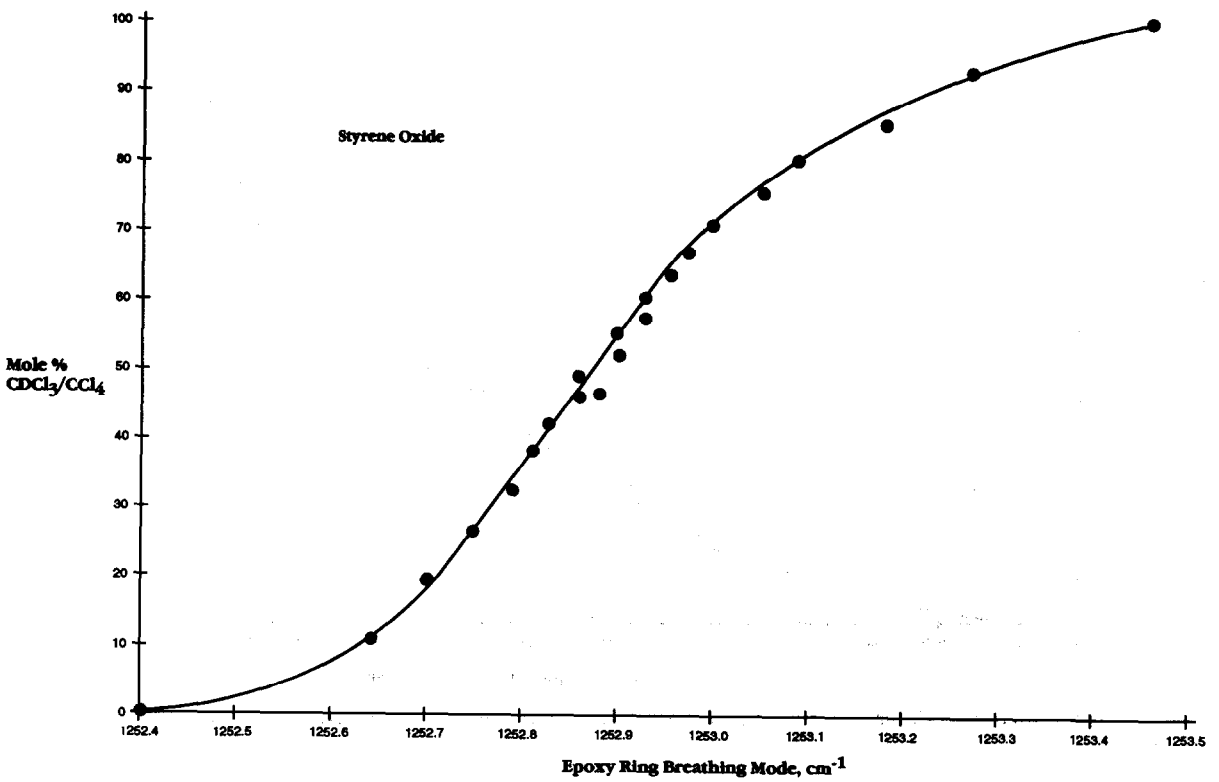

Fig. 1. A plot of the epoxy ring breathing mode for styrene oxide vs. mole% $CDCl_3/CCl_4$.

given in Tables 2 and 3, respectively. Fig. 1 shows a plot of the epoxy ring breathing mode for styrene oxide vs. mole% $CDCl_3/CCl_4$. The plot shows that this ring breathing mode increases in frequency as the mole% $CDCl_3/CCl_4$ increases. Apparent breaks in the plot near 15 and 70 mole% $CDCl_3/CCl_4$ suggest the presence of different complexes being formed between the solvent system and the free pair of electrons on the epoxy oxygen atom and with the phenyl group π system.

In the $CHCl_3/CCl_4$ solution study of acetone [7], it was shown that the ν(C=O) frequency was dependent upon both intermolecular hydrogen bonding and the reaction field of the solvent. The reaction field $[R = (\epsilon - 1)/(2\epsilon + n^2)]$ is derived from bulk dielectric theory, an ϵ is the dielectric constant of the solvent or solvent system, and n is the refractive index of the solvent or solvent system [29]. As the value of the reaction field becomes larger, there is a larger dipolar interaction between the solute and solvent in addition to the effects of hydrogen bonding. Therefore, we attribute the linear frequency shift to dipolar effects between solute and solvent, and we attribute the breaks in the plot to the presence of

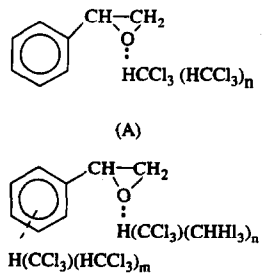

Scheme 1.

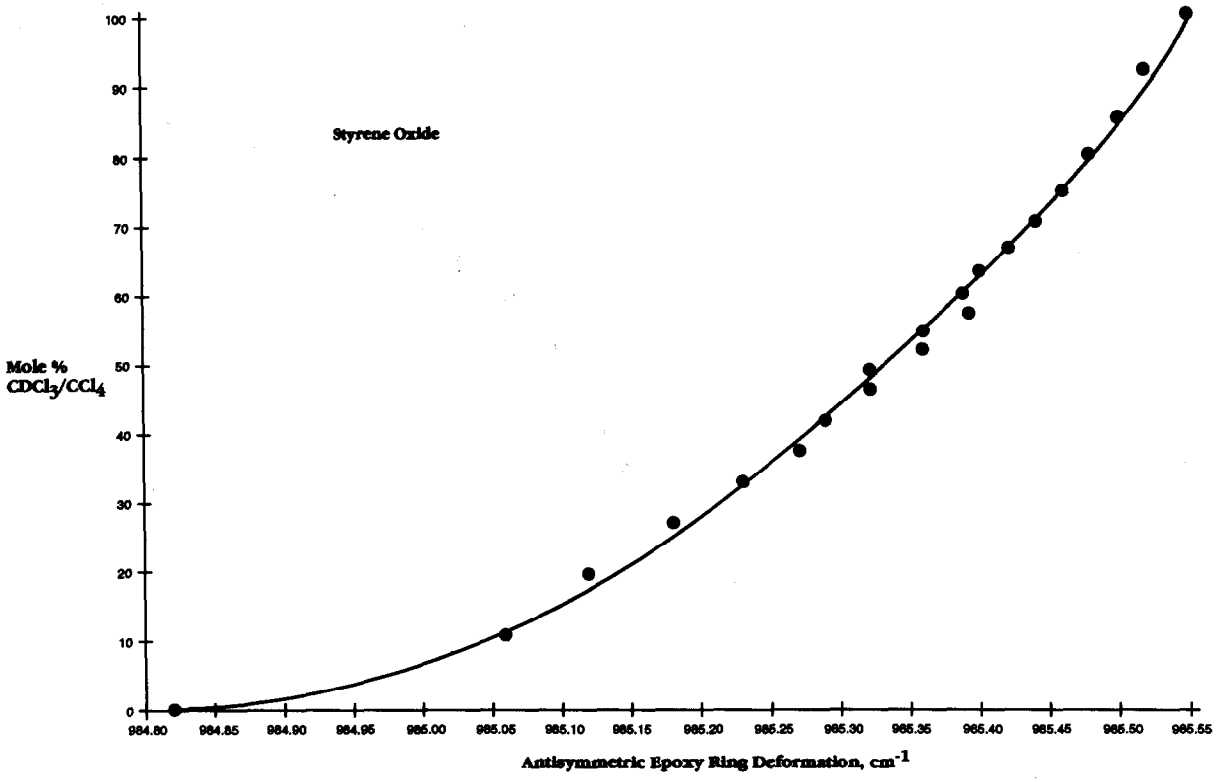

Fig. 2. A plot of the antisymmetric epoxy ring deformation for styrene oxide vs. mole% $CDCl_3/CCl_4$.

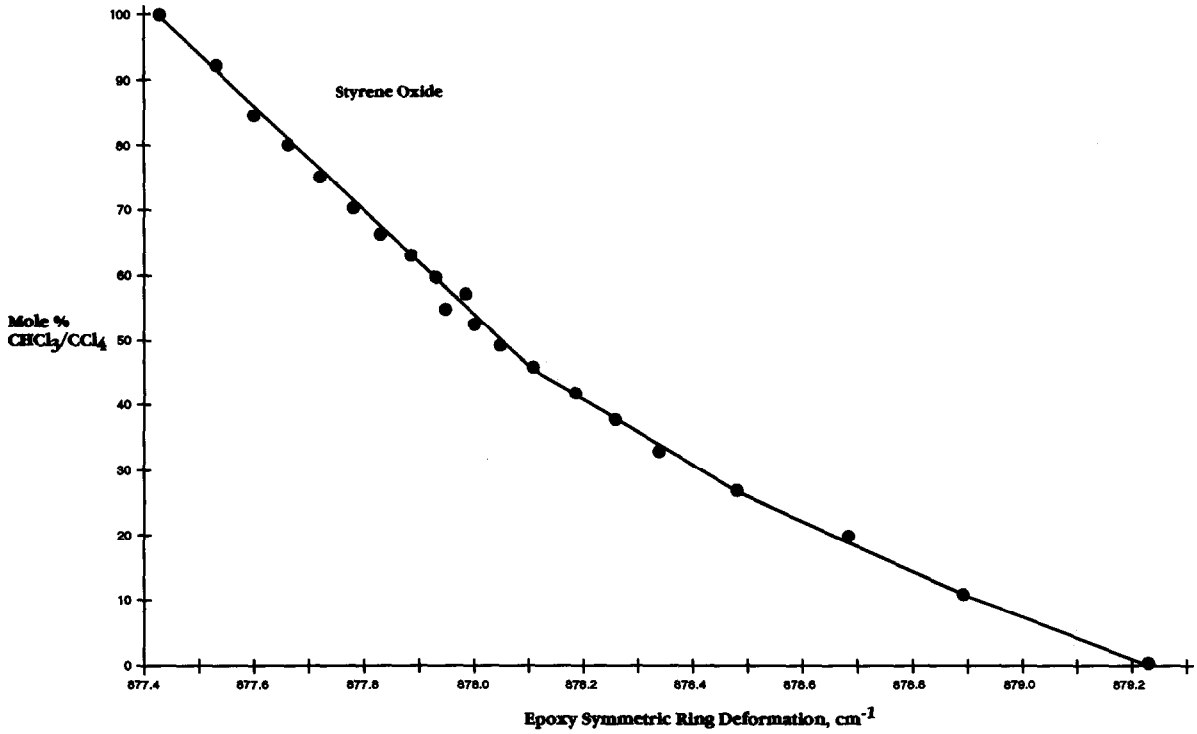

Fig. 3. A plot of the epoxy symmetric ring deformation for styrene oxide vs. mole% $CDCl_3/CCl_4$.

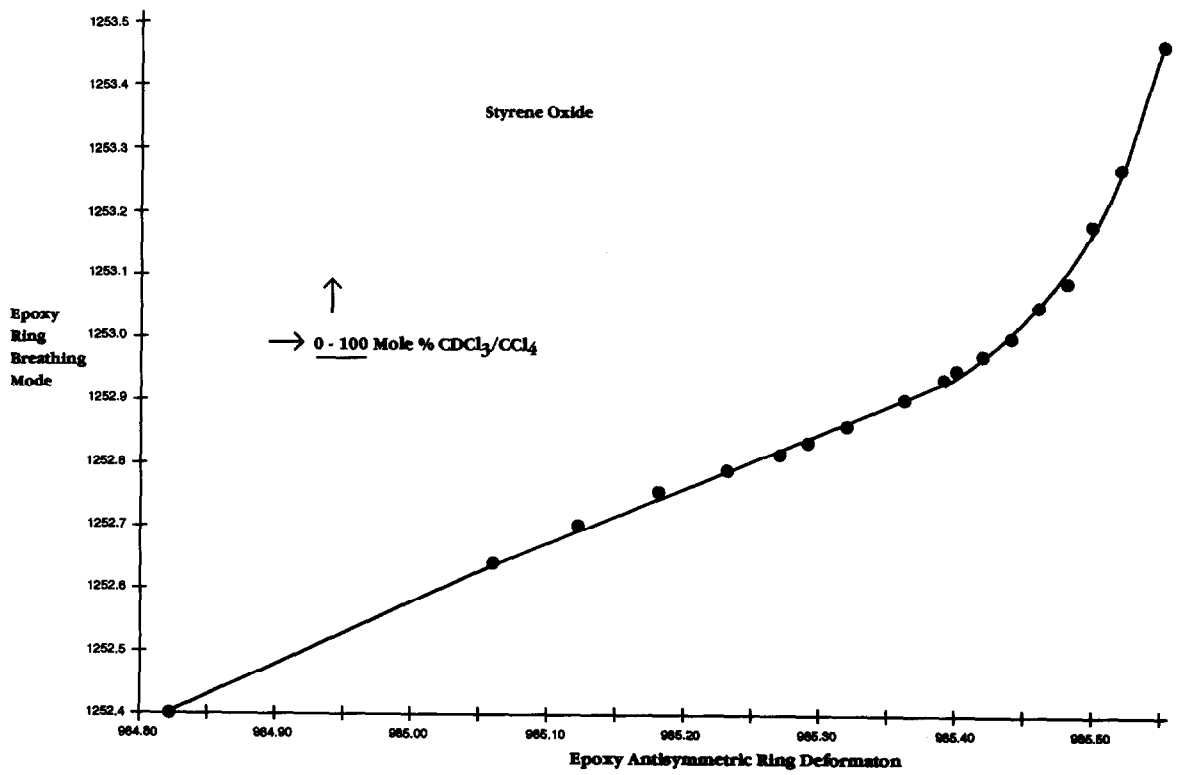

Fig. 4. A plot of the epoxy antisymmetric ring deformation vs. the epoxy ring breathing mode for styrene oxide in $CDCl_3$ and/or CCl_4 solutions.

different intermolecular hydrogen bonding species such as A and B (Scheme 1).

Fig. 2 shows a plot of the antisymmetric epoxy ring deformation for styrene oxide vs. mole% $CDCl_3/CCl_4$, and this plot shows that the antisymmetric epoxy ring deformation increases in frequency as the mole% $CDCl_3/CCl_4$ increases. Fig. 3 shows a plot of the epoxy symmetric ring deformation for styrene oxide vs. mole% $CDCl_3/CCl_4$. This plot shows that the epoxy symmetric ring deformation decreases in frequency as the mole% $CHCl_3/CCl_4$ increases. Fig. 4 shows a plot of the epoxy antisymmetric ring deformation for styrene oxide vs. the epoxy ring breathing deformation. This plot shows that both modes increase in frequency as the mole% $CDCl_3/CCl_4$ increases.

Fig. 5 shows a plot of the epoxy symmetric ring deformation vs. the epoxy antisymmetric ring deformation for styrene oxide, and this plot shows that the symmetric deformation decreases in frequency as the antisymmetric deformation increases in frequency as the mole% $CHCl_3$ or $CDCl_3/CCl_4$ increases.

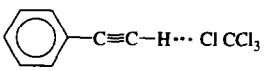

(C)

Scheme 2.

3.2. Phenylacetylene

Table 4 lists IR data for phenylacetylene in $CHCl_3/CCl_4$ solutions. Fig. 6 shows a plot of ν(≡C–H) for phenylacetylene vs. mole% $CHCl_3/CCl_4$. This plot shows that ν(≡C–H) decreases in

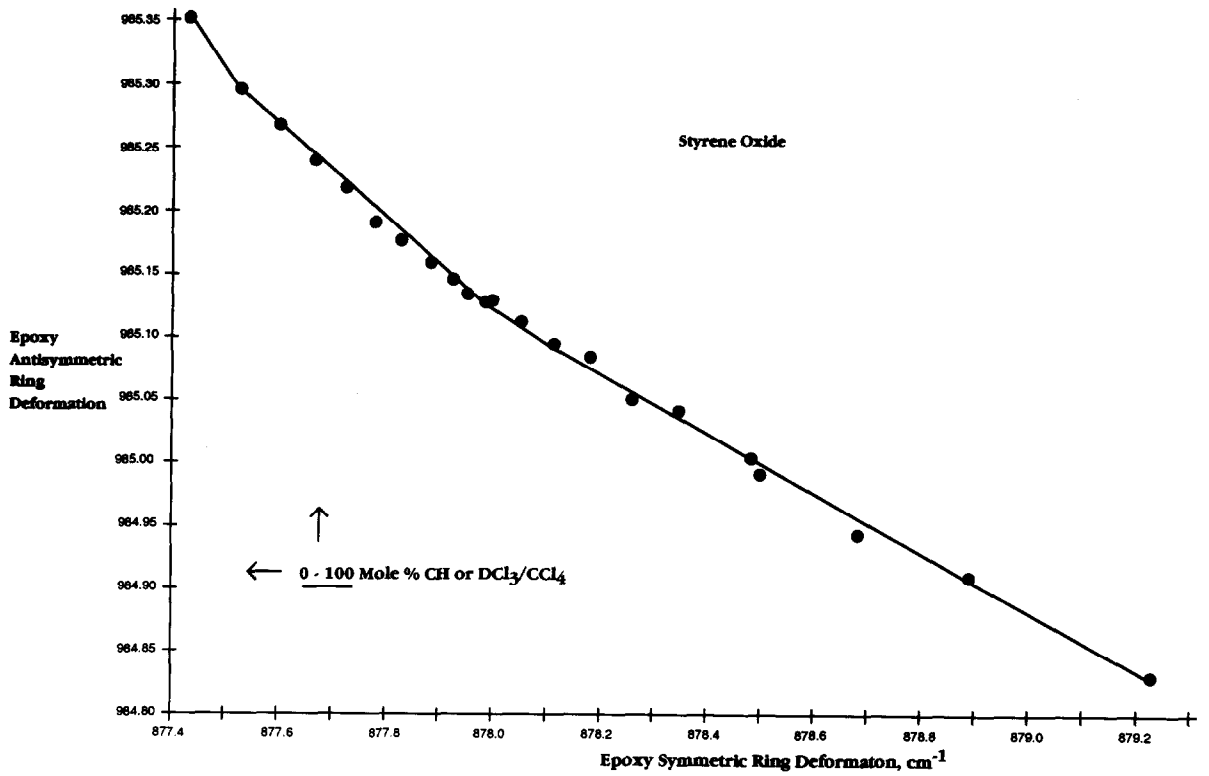

Fig. 5. A plot of the epoxy symmetric ring deformation vs. the epoxy antisymmetric ring deformation for styrene oxide in $CDCl_3$ or $CHCl_3$ and/or CCl_4 solutions.

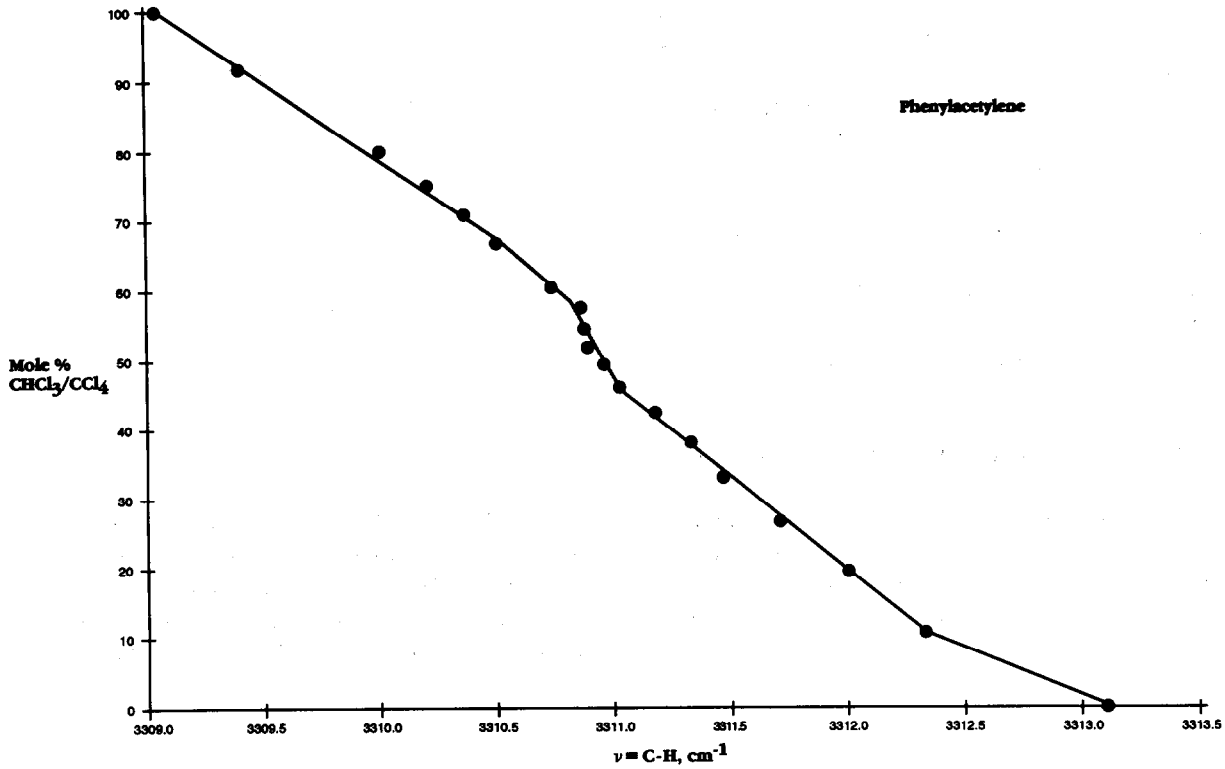

Fig. 6. A plot of $\nu(\equiv C-H)$ for phenylacetylene vs. mole% $CHCl_3/CCl_4$.

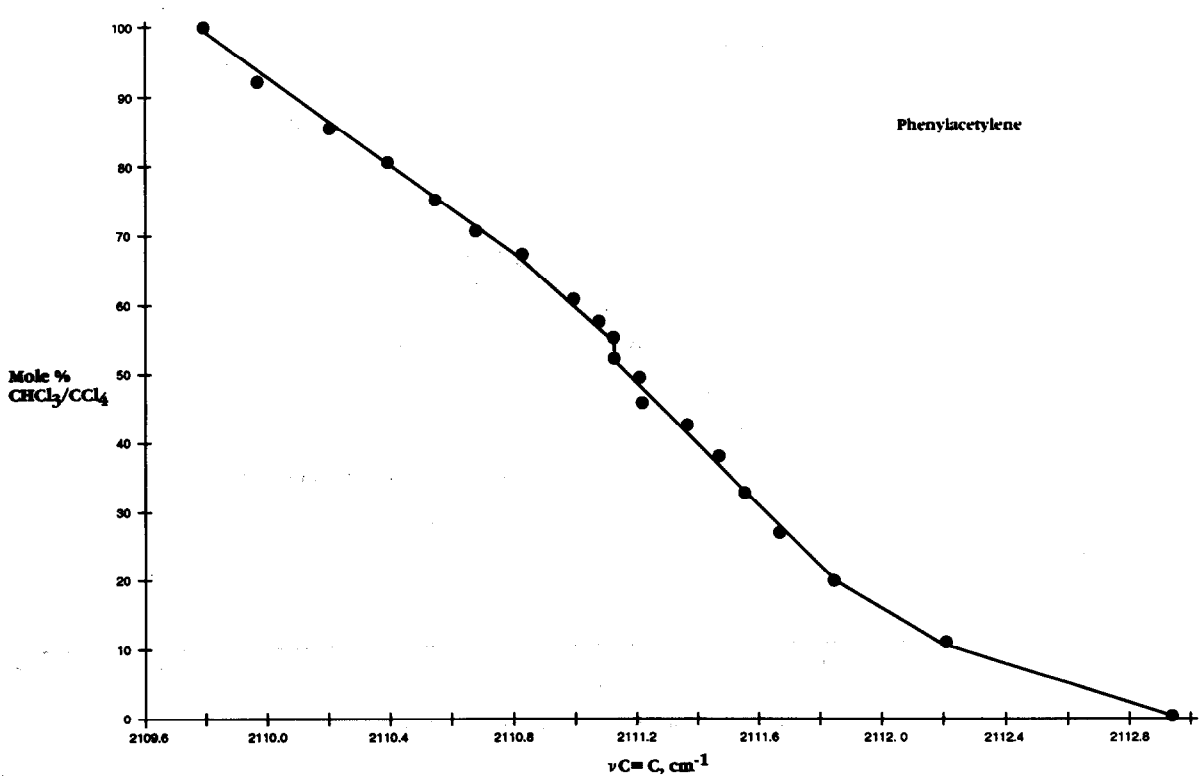

Fig. 7. A plot of $\nu(C\equiv C)$ for phenylacetylene vs. mole% $CHCl_3/CCl_4$.

frequency as the mole% $CHCl_3/CCl_4$ increases. Breaks in the plot occur near 10 and 45–55 mole% $CHCl_3/CCl_4$, which indicates that different complexes are being formed as the mole% $CHCl_3/CCl_4$ changes.

In the case of phenylacetylene in CCl_4 solution, a complex such as C (see Scheme 2) is expected.

Upon the addition of $CHCl_3$ to CCl_4, the complexes would shift from C thru E (see Scheme 3) as the mole% $CHCl_3/CCl_4$ increased from 0 to 100.

Bulk dielectric effects of the solvents also contribute to the group frequency shifts as the mole% $CHCl_3/CCl_4$ changes from 0 to 100.

Fig. 7 shows a plot of $\nu(C{\equiv}C)$ for phenylacetylene vs. mole% $CHCl_3/CCl_4$, and this plot shows that $\nu(C{\equiv}C)$ decreases in frequency as the mole% $CHCl_3/CCl_4$ increases. Fig. 8 shows a plot of $\nu({\equiv}C{-}H)$ vs. $\nu(C{\equiv}C)$ for phenylacetylene

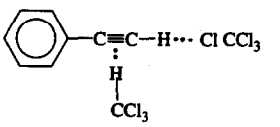

(D)

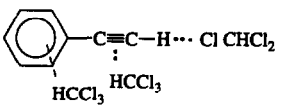

(E)

Scheme 3.

in the $CHCl_3/CCl_4$ solutions. The arrows indicate that both modes decrease in frequency as the mole% $CHCl_3/CCl_4$ increases.

Fig. 9 shows a plot of $\delta_{ip}({\equiv}C{-}H)$ for phenylacetylene vs. mole% $CHCl_3/CCl_4$. At higher

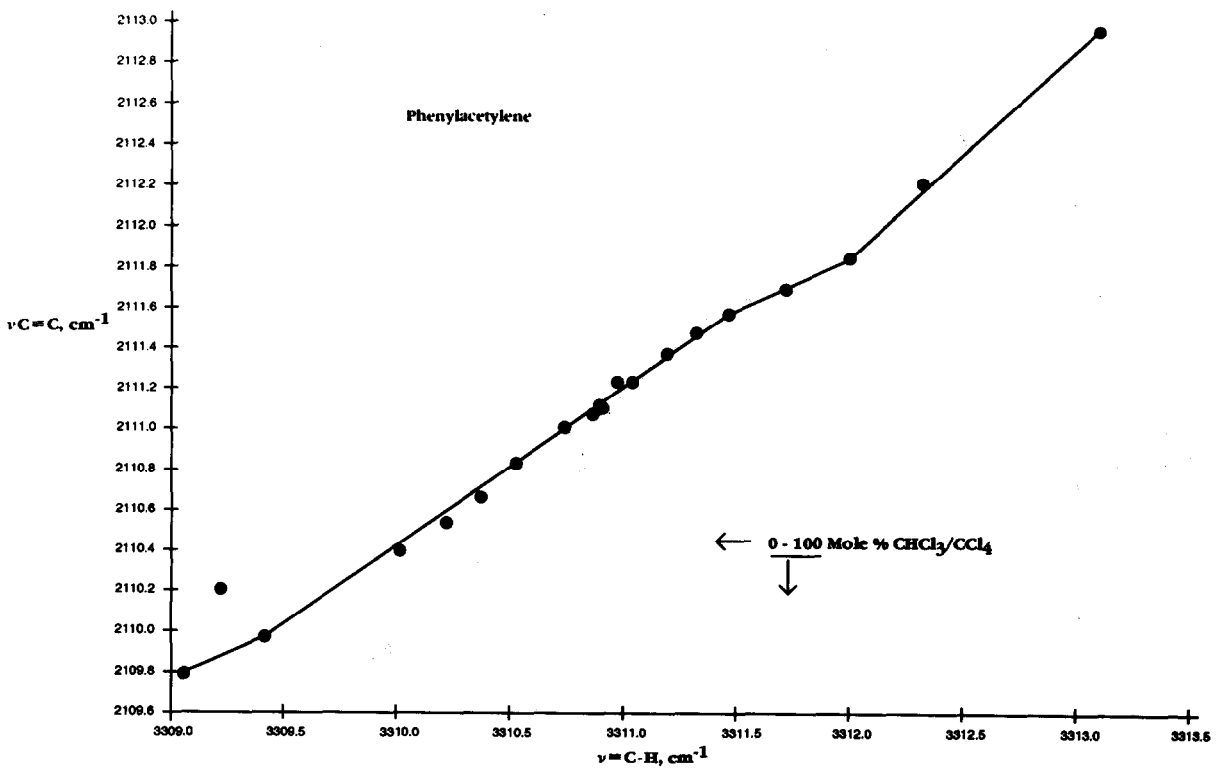

Fig. 8. A plot of $\nu(\equiv C{-}H)$ vs. $\nu(C{\equiv}C)$ for phenylacetylene in $CHCl_3$ and/or CCl_4.

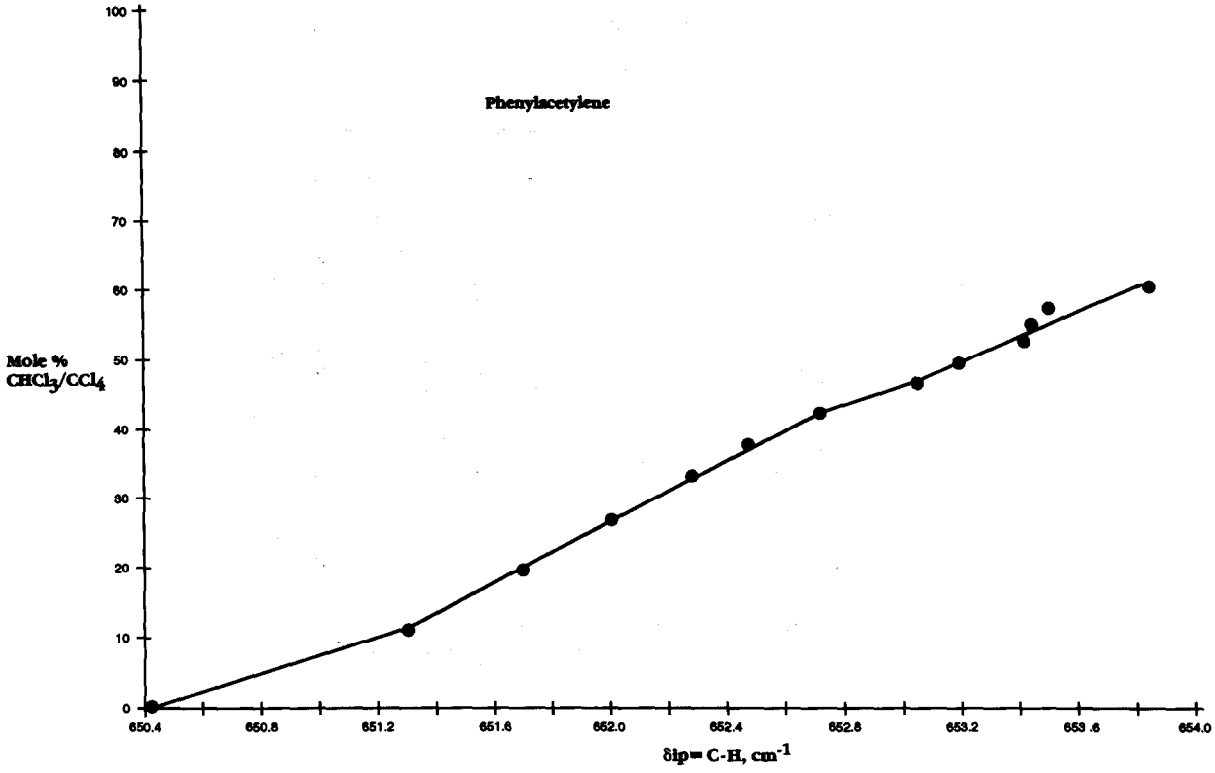

Fig. 9. A plot of δ_{ip}(≡C–H) for phenylacetylene vs. mole% $CHCl_3/CCl_4$.

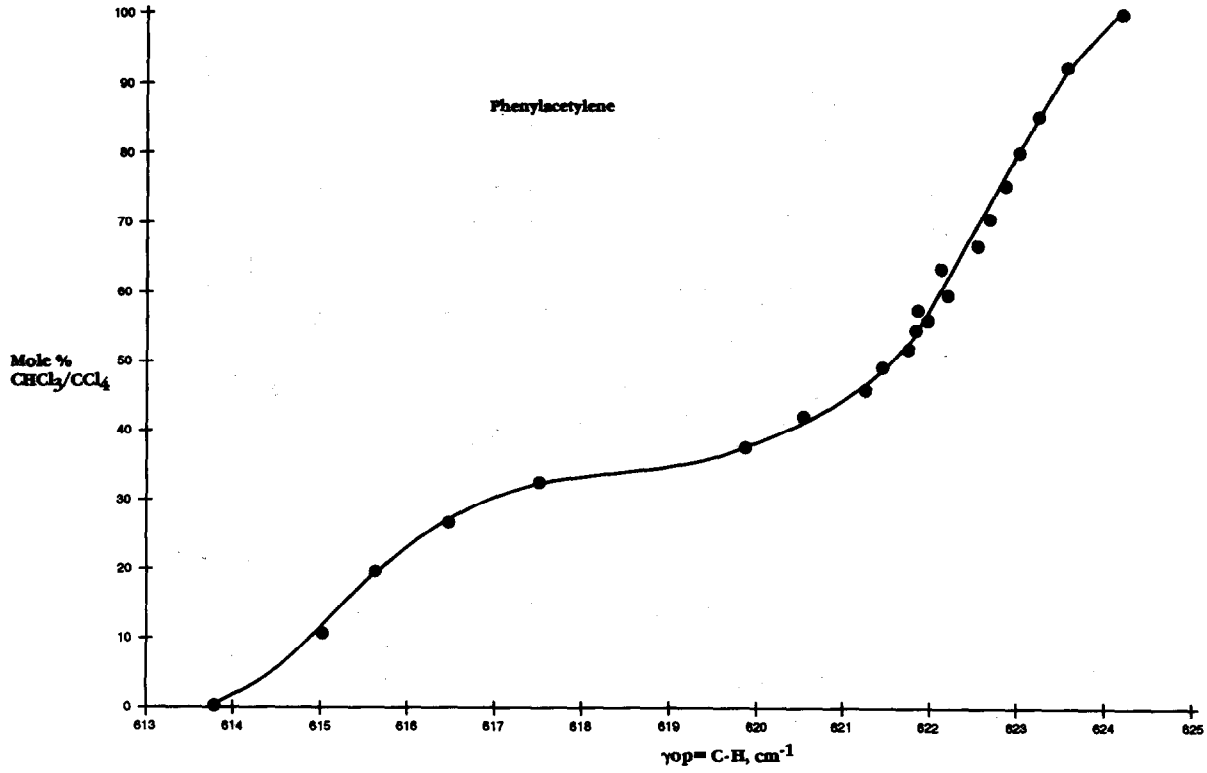

Fig. 10. A plot of γ_{op}(≡C–H) for phenylacetylene vs. mole% $CHCl_3/CCl_4$.

Table 5
Infrared data for 2% (w/v) in various solvents and in the neat liquid phase

		$\nu(\equiv C-H)$ and $[2\gamma_{op}(\equiv C-H) + \nu(C\equiv C)]$		Corrected for FR		$\nu(C\equiv H)$ (hexane) minus $\nu(C\equiv H)$ (solvent or neat)	$\nu(C\equiv C)$ $(\equiv C-H)$	δ_{ip} $(\equiv C-H)$	γ_{op} (b_2)	ν_{32} (b_2)	ν_{34} (b_1l)	ν_{24}	AN
				$\nu(C\equiv H)$	$[2\gamma_{op}(\equiv C-H) + \nu(C\equiv C)]$								
1	Hexane	3322.91	(3311.27)	3318.1	3316.1	0.0	2115.18	647.71	610.54	690.13	528.92	512.97	0
2	Diethyl ether	3320.51	(3303.93)	3313.7	3310.7	4.4	2114.04	646.42	608.96	692.23	530.46		3.9
3	Methyl *tert*-butylether	3320.89	(3304.73)	3314.7	3308.6	3.4	2109.07	646.40	608.56	692.20	530.32		4.4
4	Carbontetrachloride	3313.12	(3306.94)	3308.5	3307.0	9.6	2112.95	650.42	613.79	690.37	530.04	513.55	8.6
5	Carbondisulfide	(3307.66)	3297.81	3302.0	3303.5	16.1	2111.50	648.03	610.95	689.31	528.55	512.87	
6	Benzene	(3306.94)	3291.99	3298.6	3300.3	19.5	2110.75				530.29	513.30	8.2
7	1,2-Dichlorobenzene	(3307.46)	3296.04	3301.2	3302.3	16.9	2113.85			691.26	530.28	512.97	13.8
8	Nitrobenzene	(3303.82)	3289.21				2110.47		622.81			514.73	14.8
9													
10	Benzonitrile	(3303.25)	3287.74				2109.21					513.80	15.5
11			3275.15										
12	Nitromethane	(3304.18)	3284.96	3293.9	3300.5	24.2	2109.24			694.94	532.89	514.45	18.5
13	Methylenechloride	(3307.18)	3294.93	3300.7	3301.4	17.4	2110.91		623.57		531.03	513.61	20.4
14	Chloroform	3309.05	(3303.25)	3302.7	3301.7	15.4	2109.78		624.18	691.83	530.48	513.39	23.1
15	Chloroform-*d*	3309.20	(3299.81)				2109.81		623.01	692.51	530.57	513.70	23.1
16	*tert*-Butyl alcohol						2112.49			690.72	530.44	513.75	29.1
17	Isopropyl alcohol						2112.01			691.51	530.68	513.34	33.5
18	Ethyl alcohol						211306				532.28	513.44	37.1
19	Methyl alcohol						2111.16						41.3
20	Neat	(3305.08)	3291.17	3297.2	3299.2	20.9	2109.62	656.76	621.17	691.10	530.20	513.41	
	Δcm^{-1}	−19.66	−37.99				−6.11	10.34	15.62	5.01	4.34	1.48	

AN stands for solvent acceptor numbers.
( ) indicates shoulder of strong band and is assigned to the combination tone.
FR is Fermi resonance.

mole% $CHCl_3/CCl_4$ the absorbance from $CHCl_3$ masks δ_{ip}(≡C–H). The data show that the in-plane acetylenic carbon hydrogen bending mode, δ_{ip}(≡C–H), increases in frequency as the mole% $CHCl_3/CCl_4$ increases. Fig. 10 shows a plot of the out-of-plane carbon hydrogen bending mode, γ_{op}(≡C–H), for phenylacetylene vs. mole% $CHCl_3/CCl_4$ and the plot shows that γ_{op}(≡C–H) increases in frequency as the mole% $CHCl_3/CCl_4$ increases. This γ_{op}(≡C–H) mode shows breaks in the curve similar to that shown in Fig. 9 for δ_{ip}(≡C–H) vs. mole% $CHCl_3/CCl_4$. Fig. 11 shows a plot of ν(≡C–H) vs. γ_{op}(≡C–H) for phenylacetylene in the $CHCl_3/CCl_4$ solutions. The arrows indicate that the ν(≡C–H) mode decreases in frequency while the γ_{op}(≡C–H) mode increases in frequency as the mole% $CHCl_3/CCl_4$ increases.

Fig. 12 shows a plot of ν_{32} (b_2) phenyl ring out-of-plane deformation for phenylacetylene vs. the mole% $CHCl_3/CCl_4$. This plot shows that the ν_{32} (b_2) mode increases in frequency as the mole% $CHCl_3/CCl_4$ increases. Fig. 13 shows a plot of ν_{24} (b_1) phenyl ring skeletal deformation and the ν_{34} (b_2) phenyl ring skeletal deformation for phenylacetylene vs. the mole% $CHCl_3/CCl_4$. The ν_{24} (b_1) mode decreases in frequency while the ν_{34} (b_2) mode increases in frequency as the mole% $CHCl_3/CCl_4$ increases. The three phenyl ring modes discussed in Figs. 12 and 13 are not affected as much as the modes for the C≡C–H group are affected by change in the mole% $CHCl_3/CCl_4$.

Table 5 lists IR data for 2 wt.% phenylacetylene in various solvents and as a neat liquid.

Two IR bands are noted near 3300 cm^{-1} in the neat liquid phase and in the 2% (w/v) phenylacetylene solutions using various solvents. For example, in solution in hexane, the strongest band in this set occurs at 3322.91 cm^{-1} and the shoulder occurs at 3311.27 cm^{-1}, while in the neat liquid phase the strongest band in this set

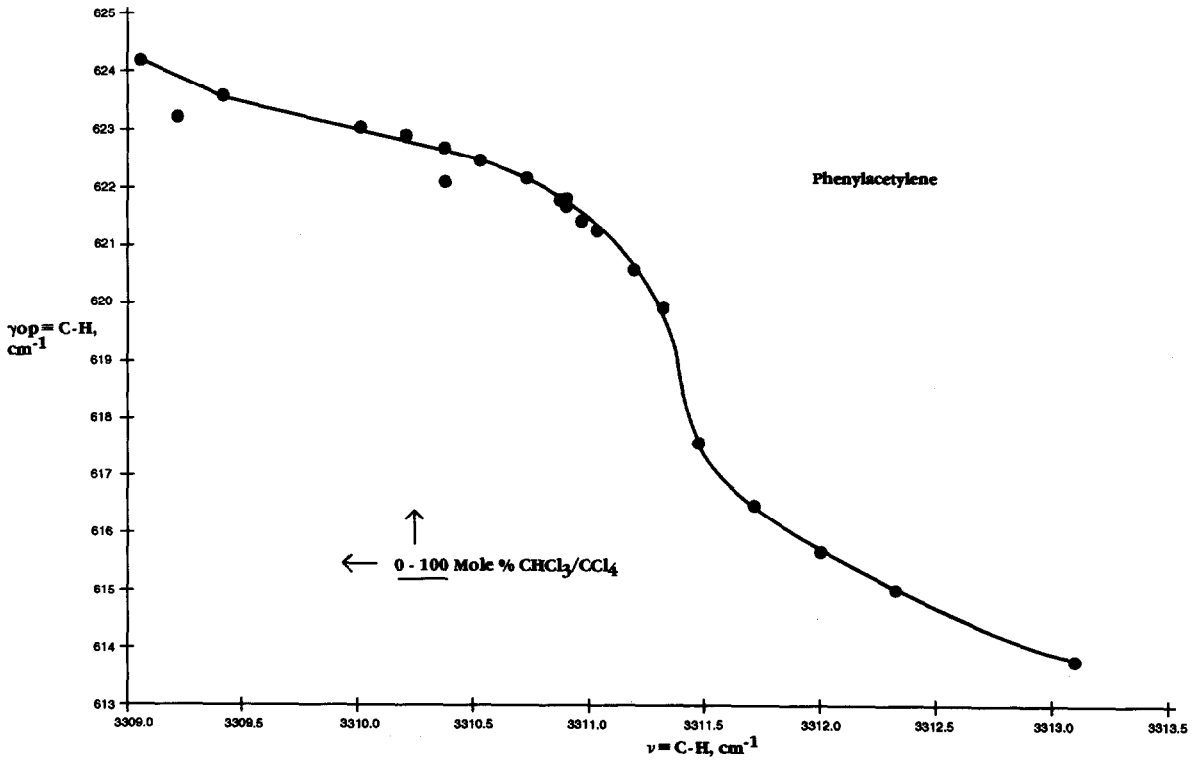

Fig. 11. A plot of ν(≡C–H) vs. γ_{op}(≡C–H) for phenylacetylene in $CHCl_3$ and/or CCl_4 solutions.

occurs at 3291.17 cm^{-1} and the shoulder occurs at 3305.08 cm^{-1}. Using carbon disulfide as the solvent, the strongest band in this set occurs at 3297.81 cm^{-1} and the shoulder occurs at 3307.66 cm^{-1}. The shoulder on ν(≡C–H) for phenylacetylene has been assigned to the combination tone [ν(C≡C) + $2\gamma_{op}$(≡C–H)] [4]. The frequency and intensity changes of these two bands suggest that the ν(≡C–H), a' mode and the combination tone [$2\gamma_{op}$(≡C–H) + ν(C≡C), a'] are in Fermi resonance (FR), and we have corrected these modes for FR. The ν(≡C–H) mode decreases 20.9 cm^{-1} in going from solution in hexane to the neat liquid phase while the ν(≡C–H) mode decreases 17.4 cm^{-1} in going from solution in hexane to solution $CHCl_3$, and decreases 16.1 cm^{-1} in going from solution in hexane to solution in CS_2. The larger the decrease in frequency for ν(≡C–H) for phenylacetylene in going from solution in hexane to solution in another solvent, the stronger the intermolecular bonding between the acetylenic C–H group and a basic site of the solvent or the most basic site in phenylacetylene. These data do not correlate well with the solvent acceptor number (AN) of the solvent, and this may be due to the fact that the AN values do not reflect the intermolecular hydrogen bonding capability of the solvents such as CH_2Cl_2 and $CHCl_3$.

The ν(C≡C) mode for phenylacetylene occurs in the region 2109.07–2115.18 cm^{-1} in various solvents. The ν(C≡C) frequencies do not correlate with the solvent AN values. The in-plane acetylenic ≡C–H bending mode, δ_{ip}(≡C–H) for

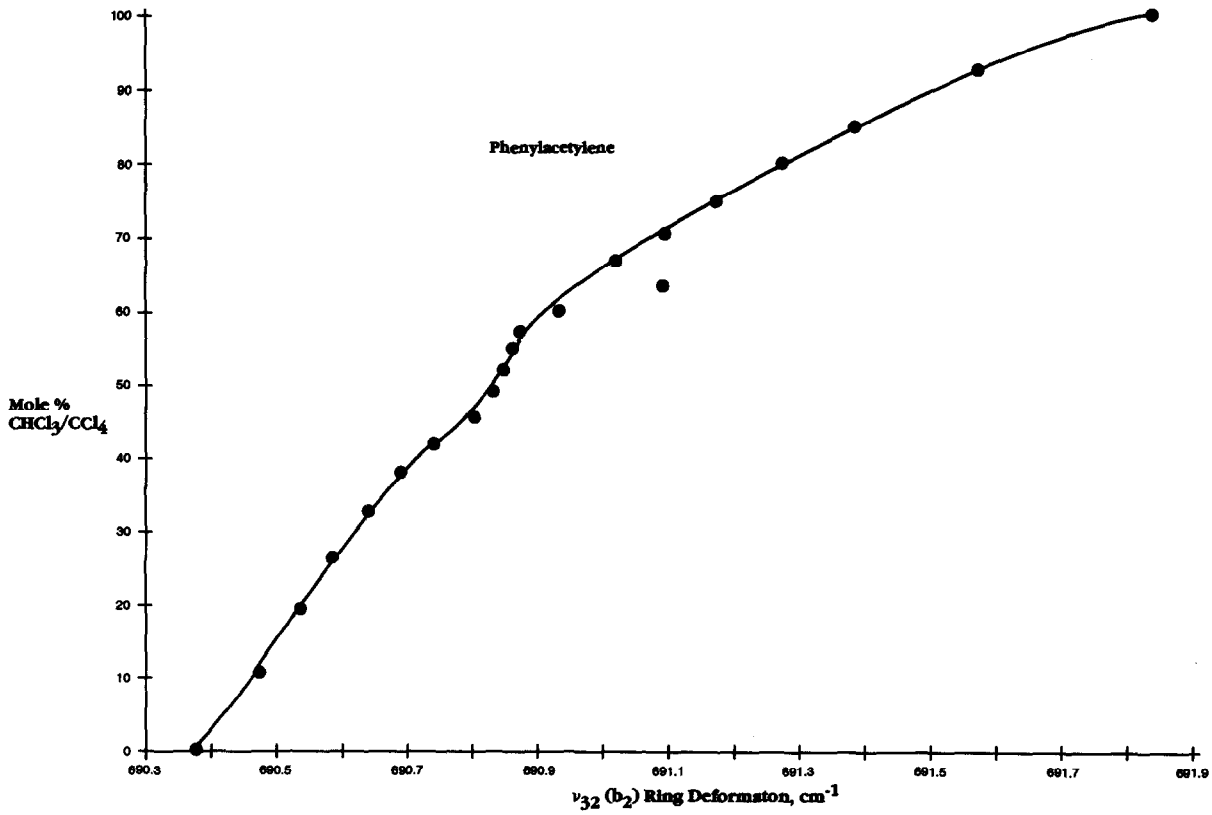

Fig. 12. A plot of an out-of-plane phenylacetylene deformation, ν_{32} (b_2) for phenylacetylene vs. mole% $CHCl_3/CCl_4$.

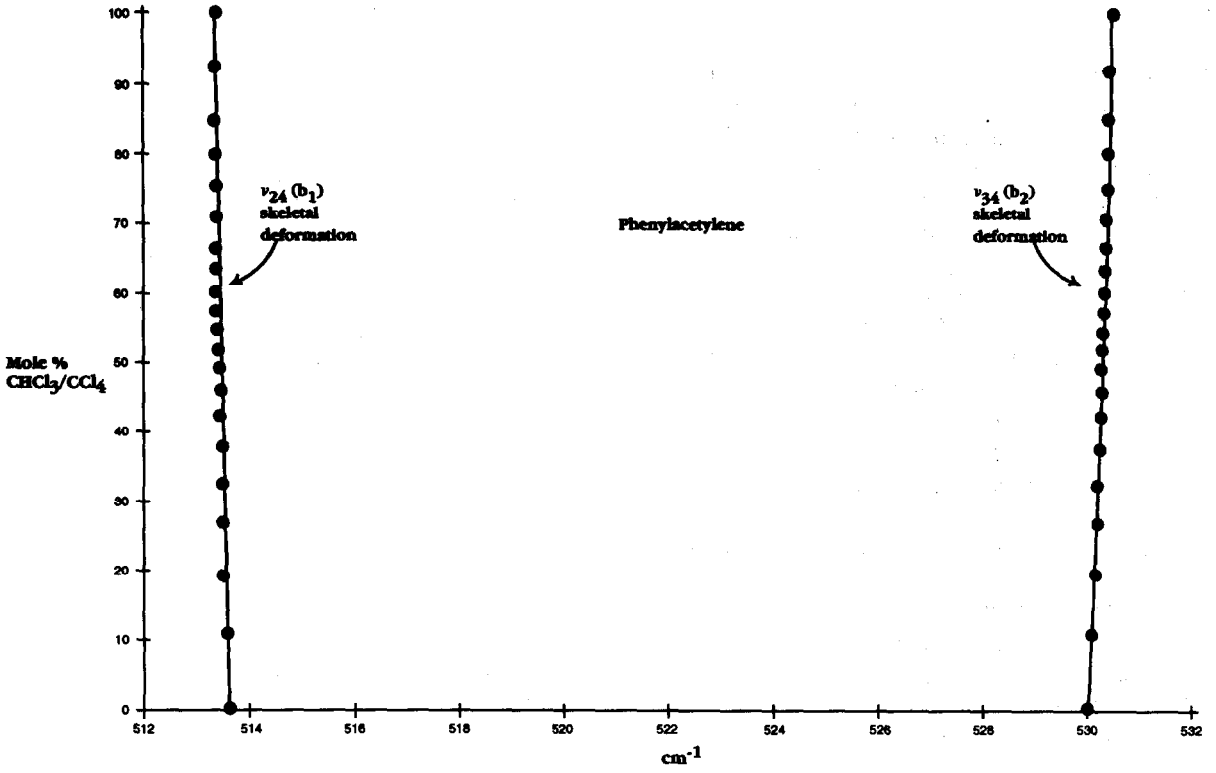

Fig. 13. A plot of an in-plane phenyl ring skeletal deformation, ν_{24} (b_1) vs. mole% $CHCl_3/CCl_4$ and a plot of an out-of-plane skeletal deformation, ν_{34} (b_2) vs. mole% $CHCl_3/CCl_4$.

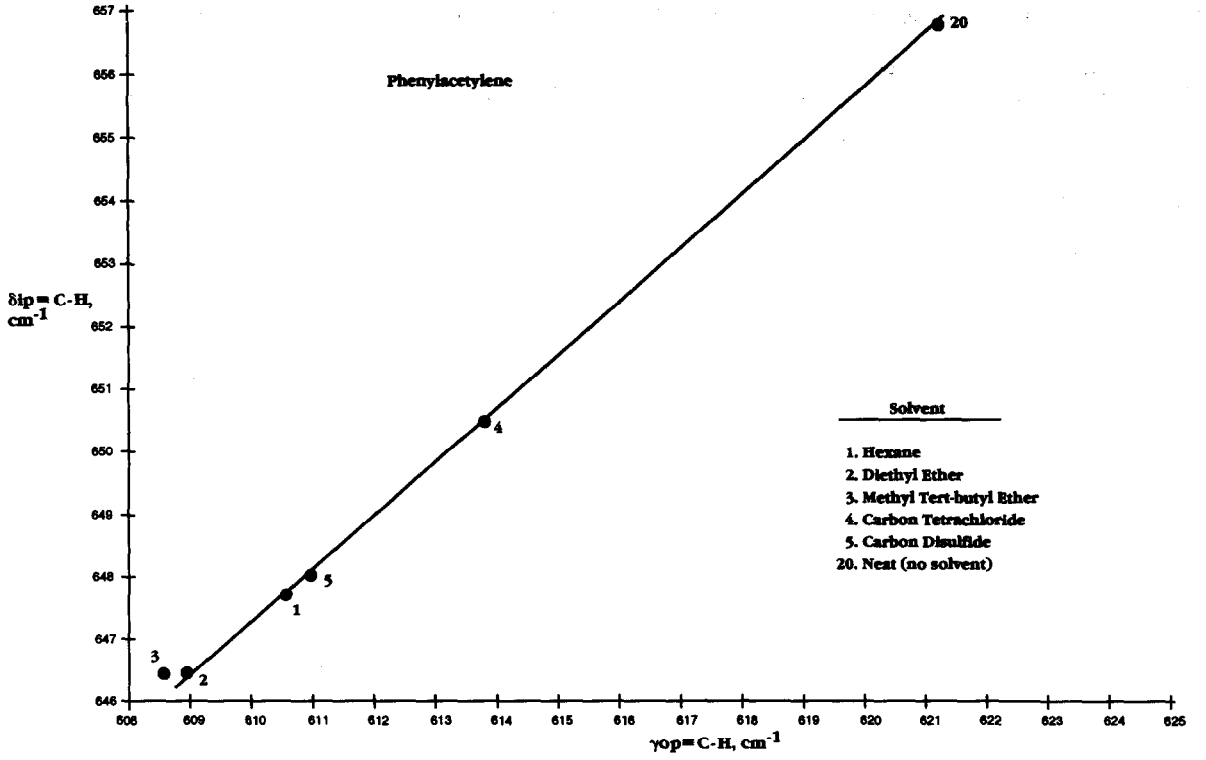

Fig. 14. A plot of γ_{op}(≡C–H) vs. δ_{ip}(≡C–H) for phenylacetylene in the neat liquid phase and in solution in various solvents.

phenylacetylene, is masked by most of the solvents used in this study. In the neat liquid phase δ_{ip}(≡C–H) is assigned at 656.76 cm^{-1} and occurs at 647.71 cm^{-1} in hexane solution.

The out-of-plane ≡C–H bending mode, γ_{op}≡C–H) for phenylacetylene occurs at 621.17 cm^{-1} in the neat liquid phase and occurs at 610.54 cm^{-1} in hexane solution. Fig. 14 is a plot of γ_{op}(≡C–H) vs. δ_{ip}(≡C–H) for phenylacetylene in the neat liquid phase and in solution with five different solvents. The plot is apparently linear. On this basis one would expect δ_{ip}(≡C–H) for phenylacetylene in separate solution with nitrobenzene, methylene chloride, or chloroform to occur above 657 cm^{-1}.

The ν_{32} (b_2) mode occurs in the region 689.31–695.14 cm^{-1}, the ν_{34} (b_2) mode occurs in the region 528.55–532.89 cm^{-1}, and the ν_{24} (b_1) mode occurs in the region 512.87–514.73 cm^{-1} for phenylacetylene in the solvents used in this study [4]. The three ring modes are affected less than those modes arising within the C≡C–H group.

References

[1] R.A. Nyquist and C.L. Putzig, Appl. Spectrosc., 40 (1986) 112.
[2] R.A. Nyquist, Appl. Spectrosc., 40 (1986) 275.
[3] R.A. Nyquist, C.L. Putzig and N.E. Skelly, Appl. Spectrosc., 40 (1986) 821.
[4] J.C. Evans and R.A. Nyquist, Appl. Spectrosc., 16 (1960) 918.
[5] R.A. Nyquist, V. Chrzan and J. Houck, Appl. Spectrosc., 43 (1989) 981.
[6] R.A. Nyquist, C.L. Putzig and L. Yurga, Appl. Spectrosc., 43 (1989) 983.
[7] R.A. Nyquist, C.L. Putzig and D.L. Hasha, Appl. Spectrosc., 43 (1989) 1049.
[8] R.A. Nyquist, T.M. Kirchner and H.A. Fouchea, Appl. Spectrosc., 43 (1989) 1053.
[9] R.A. Nyquist, Appl. Spectrosc., 43 (1989) 1208.
[10] R.A. Nyquist, Appl. Spectrosc., 43 (1989) 1374.
[11] R.A. Nyquist, V. Chrzan T.M. Kirchner, L. Yurga and C.L. Putzig, Appl. Spectrosc., 44 (1990) 243.
[12] R.A. Nyquist, Appl. Spectrosc., 44 (1990) 426.
[13] R.A. Nyquist, Appl. Spectrosc., 44 (1990) 433.
[14] R.A. Nyquist, Appl. Spectrosc., 44 (1990) 438.
[15] R.A. Nyquist, Appl. Spectrosc., 44 (1990) 594.
[16] R.A. Nyquist, Appl. Spectrosc., 44 (1990) 783.
[17] R.A. Nyquist and S.E. Settineri, Appl. Spectrosc., 44 (1990) 791.
[18] R.A. Nyquist, Appl. Spectrosc., 44 (1990) 1405.
[19] R.A. Nyquist and S.E. Settineri, Appl. Spectrosc., 44 (1990) 1552.
[20] R.A. Nyquist and S.E. Settineri, Appl. Spectrosc., 44 (1990) 1629.
[21] R.A. Nyquist, H.A. Fouchea, G.A. Hoffman and D.L. Hasha, Appl. Spectrosc., 45 (1991) 860.
[22] R.A. Nyquist and S.E. Settineri, Appl. Spectrosc., 45 (1991) 1075.
[23] R.A. Nyquist and D.A. Luoma, Appl. Spectrosc., 45 (1991) 1491.
[24] R.A. Nyquist and D.A. Luoma, Appl. Spectrosc., 45 (1991) 1497.
[25] R.A. Nyquist, Appl. Spectrosc., 46 (1992) 306.
[26] R.A. Nyquist and D.A. Luoma, Appl. Spectrosc., 45 (1991) 1501.
[27] R.A. Nyquist, S.E. Settineri and D.A. Luoma, Appl. Spectrosc., 45 (1991) 1641.
[28] R.A. Nyquist, Vib. Spectrosc., 2 (1991) 221.
[29] A.D. Buckingham, Can. J. Chem., 308 (1960) 300.